Lamellar Arrangements of Linear Polyethylene in Ultrathin Films

Euntaek Woo,[1] Manshik Park,[1] Young Gyu Jeong,[2] Kyusoon Shin[1]

[1]*School of Chemical and Biological Engineering, Seoul National University, Seoul 151-744, Republic of Korea*
[2]*Department of Materials Design Engineering, Kumoh National Institute of Technology, Gumi 730-701, Republic of Korea*

Received 4 March 2011; accepted 21 August 2011
DOI 10.1002/app.35508
Published online 11 October 2011 in Wiley Online Library (wileyonlinelibrary.com).

ABSTRACT: The crystal orientations of linear polyethylene films on silicon substrates are investigated using grazing incidence X-ray diffraction and atomic force microscopy. From diffraction analysis, we can identify the structural arrangement of PE crystals in ultrathin film. The orientation of lamellar crystal in PE films changes from edge-on to flat-on with the decrease of film thickness in the film thickness below $\sim$ 100 nm. The slightly inclined lamellae relative to the substrate are found to coexist with the flat-on lamellae in thin PE films that we have investigated. We find that the crystal orientation and structures is governed by the constraint imposed by film thickness rather than enthalpy gain as the film got thinner especially in the thickness below 200 nm. © 2011 Wiley Periodicals, Inc. J Appl Polym Sci 123: 2558–2565, 2012

Key words: crystal structures; grazing incidence X-ray diffraction; polyethylene; thin films

INTRODUCTION

The structure of polymers confined to thin and ultrathin films have been extensively studied during the recent decades in polymer science and technology[1–9] The chain packing of polymers in films is a factor in tuning the properties for various practical applications such as organic electronics and surface coatings.[1,4] Studies on thin films have been performed on amorphous glassy polymers[5–7] as well as semicrystalline polymers.[1–3,10–14] Among those studies, understanding the crystalline structures and orientations in thin crystalline polymer films would be fundamentally important and at the same time useful in the practical applications of crystalline polymer-based thin films such as organic optoelectronic devices.[8,9]

Several groups have studied the crystallization behaviors and structures of semicrystalline polymers confined to nanoscopic spaces.[1–3,10–33] Frank and coworkers[1–3] reported the substantial reduction of the crystallization rate in ultrathin films of poly(di-*n*-hexylsilane). Mellbring et al.[10] observed a morphological change from spherulitic structure to aggregated edge-on lamellae structure, as the thickness of as-cast polyethylene (PE) films decreases. Recently, studies on the change of lamellar orientation depending on the film thickness were reported for the thin and ultrathin films of poly(di-*n*-hexylsilane),[11] linear low-density PE,[12] and poly(ethylene oxide).[13] Yang and coworkers observed windmill-like morphology with twisted lamellae.[14] One of important factors in governing the crystallization behavior and structure in thin film must be surface or interfacial free energy. The formation of edge-on lamella orientation is known to be the result of the crystallization with the energetic benefit of substrate surface.[33] Entropic penalty, driven by film thickness or degree of confinement, is thought to be another one that could explain the kinetic formation of flat-on lamella.

Despite the many efforts, however, the polymer crystallization on flat substrates, occurring even under a severe confinement, still makes it challenging to control micro- and nano-structural evolution and resulting properties of the thin films. To this end, it is necessarily preceded to investigate the crystalline structure in detail. Although the methods used in previous studies for structure determination by spectroscopy and microscopy can give the information on the orientation of crystalline polymer chains in the films, much more detailed information on the structure of polymer crystal is still highly demanded. In this study, to investigate the confinement-induced structure of the thin

Correspondence to: K. Shin (shin@snu.ac.kr).
Contract grant sponsor: Korea Ministry of Environment; contract grant number: 102-081-067.
Contract grant sponsor: Ministry of Land, Transportation, and Maritime Affairs (MLTM) of Korean Government; contract grant number: 09CCTI-B050566-02-000000.
Contract grant sponsor: Nano R&D Program, Korean Government; contract grant number: 2010-0019111.

polymeric films in detail, we have characterized the crystal orientation and morphological features of PE films on silicon substrates. Especially grazing incidence X-ray diffraction (GIXRD), combined with atomic force microscopy (AFM), enabled us to study on the structure and the crystal orientation of PE crystals in ultrathin film. With the aid of GIXRD and AFM, we found that slightly inclined flat on lamellae and flat-on lamellae could coexist in PE thin film with a certain thickness. It must be also interesting and worthy to understand the formation of crystalline structure and thin film morphology of crystalline polymer in the light of energetic or entropic aspects of crystalline structure.

EXPERIMENTAL

Materials and sample preparation

A linear PE (HDPE, ME6000, $\rho = 0.961$ g cm^{-3}, $T_m = 133$°C, $M_n = 35$ kg mol^{-1}, and $M_w/M_n = 4.02$) was purchased from LG Chemical. Si ⟨100⟩ wafers were used as a substrate for PE films. The wafers were cut into squares (1.5×1.5 cm^2).

The linear PE films with various thicknesses of 21 nm to 1.2 μm were prepared by spin-casting PE in xylene solution onto the wafers. To avoid the crystallization of PE during spin-casting, the solution, dispensers, and wafers were preheated to the deposition temperature. Before spin-casting, the native oxide layer was etched by dipping the Si wafer in dilute hydrofluoric acid (48% HF : $H_2O = 1 : 10$) for 1 min. After the removal of oxide layer, the wafers were subsequently rinsed with deionized water. The spin-casting temperature was controlled to be 120°C by using a home-made heating chamber. The whole spin-casting process was performed within 1 min after HF etching to minimize the oxidation of the Si substrates. The thickness of the crystalline polymer film was controlled by the variation of concentration of the PE solution and the spinning rate, while the temperature of the chamber and the solution was kept the same. The PE films, cast on Si substrates, were melted at 145°C for 30 min on a hotplate and then recrystallized by slow cooling to 30°C at a rate of ~ 0.5°C min^{-1} in a vacuum oven. The thickness of PE films crystallized on Si wafer substrates was measured with an atomic force microscope (D3100, Veeco Instruments, USA). After scratching and scraping out the PE film piece with a razor blade, the thicknesses of the films were measured from the height difference between exposed bare wafer area and PE film surface in the scanned cross-sectional profiles.

Structural characterization

The crystalline structure and orientation in the films were determined by GIXRD. The experiments were performed using a synchrotron radiation source at 4C2 beamline of Pohang Light Source (PLS, acceleration voltage $\sim$ 2.5 GeV), Pohang, Korea. The diffracted patterns were recorded by a 2D area detector. The beam was monochromatized using a double Si (111) crystal and focused onto the sample. Beam size was 1.0×0.5 mm^2 (vertical $\times$ horizontal), and the wavelength of the beam was 1.3807 Å. The incident angle (α_i) was evaluated to be 0.12°–0.15° for thinner films (thickness $\leq$ 52 nm), and 0.14°–0.17° for thicker films (thickness >100 nm). The total acquisition time was 60 s for all samples. Sample-to-detector distance was about 16.9 cm, and the photon flux was informed to be $\sim 10^{11}$ photons/sec/mrad/0.1%. All the patterns were calibrated by silver behenate ($d = 5.84$ nm). The samples were kept under vacuum to reduce air scattering and to minimize the sample damage by X-ray radiation. Three slits were placed in front of sample stage, and the last slit was placed close to the sample so that parasitic scattering could be minimized. Innova Scanning Probe Microscope (Veeco Instruments, USA) was used in contact mode to characterize the morphological features of the PE film surfaces. The topological measurement was carried out with constant positioning of tip and 1D bow motioning of sample. The resolution was 256 $\times$ 256 pixels, and image compensation with 1D bow type was performed after measurement.

RESULTS AND DISCUSSION

The 2D GIXRD patterns of the linear PE films and bulk are shown in Figure 1(a–g). The calculated penetration depth is 1.7 μm at $\alpha_i = 0.155$°. Hence we believed that we could get the structural information for the most part of the films with the current experimental setup. As shown in Figure 1(a), the bulk PE showed typical diffraction patterns of isotropic PE crystals. The two semicircles from the center of the pattern correspond to (110) and (200) reflections of the orthorhombic PE crystals.[21] The higher order reflections were not distinctive enough for the analysis.

The (200) reflections in the GIXRD patterns showed that the PE crystals in the thin films have different orientation depending upon the variation of film thickness. The concentration of the PE solution and the spinning rate of each film for spin-casting was (a) 6.0 wt % and 3000 rpm, (b) 3.0 wt % and 3000 rpm, (c) 1.6 wt % and 3000 rpm, (d) 0.8 wt %, and 3000 rpm, (e) 0.6 wt % and 3000 rpm, and (f) 0.2 wt % and 2500 rpm, respectively. The thickness of each film was found to be (a) 1.2 μm, (b) 607 nm, (c) 255 nm, (d) 115 nm, (e) 52 nm, and (f) 21 nm, respectively, from the cross-sectional analysis of AFM after scraping out the film with a razor blade. The thickness of bulk sample was measured to be

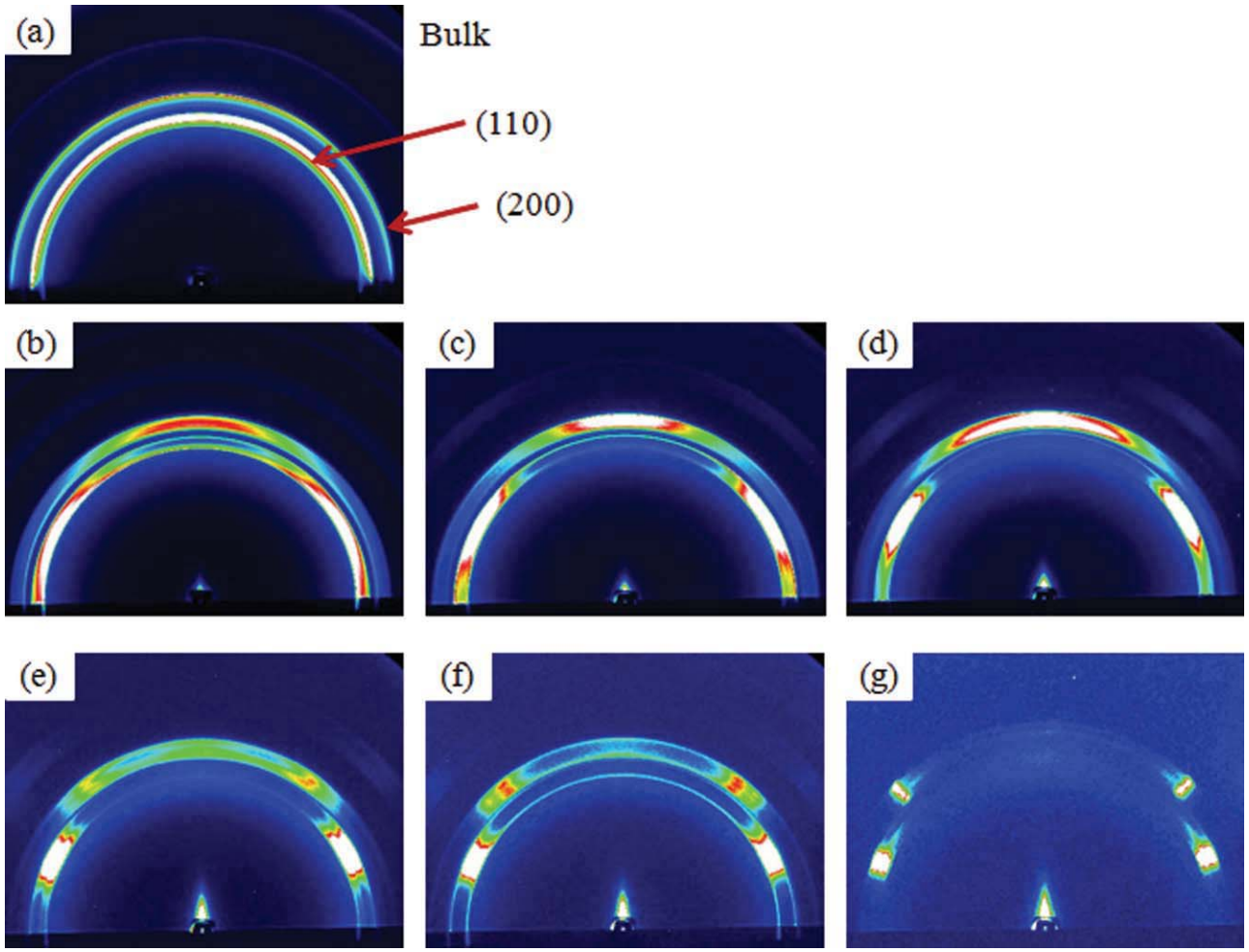

Figure 1 GIXD patterns of linear PE bulk (a) and films (b)–(h) on Si ⟨100⟩ wafers. The concentration of the PE in xylene and the spinning rate of each film for spin-coating was (b) 6.0 wt % and 3000 rpm, (c) 3.0 wt % and 3000 rpm, (d) 1.6 wt % and 3000 rpm, (e) 0.8 wt % and 3000 rpm, (f) 0.6 wt % and 3000 rpm, and (g) 0.2 wt % and 2500 rpm, respectively. The thickness of each film was measured to be (b) 1.2 μm, (c) 607 nm, (d) 255 nm, (e) 115 nm, (f) 52 nm, and (g) 21 nm, respectively. [Color figure can be viewed in the online issue, which is available at wileyonlinelibrary.com.]

about 65 μm. The arc of (200) reflections in the GIXRD patterns of thicker films appeared around the vertical center in the detector (azimuthal angle of 0°), as shown in Figure 1(b–d). It indicates that the *a* axes of the orthorhombic PE crystals are mostly aligned along the direction normal to the substrate plane with a distribution of the crystal orientation around the preferential direction, as reported by Bartczak et al.[25] From the GIXRD patterns of these films, as in Figure 1(b–d), (200) reflection appears more intense on the vertical center in the arc, as compared to bulk. In these films, the crystals more orient along their preferred direction as the film becomes thinner [Fig. 1(b,c)]. From Figure 1(c,d), the distribution of the crystal orientation becomes broader.

The preferred orientation of the PE crystal changes dramatically in much thinner films. From the reflection of (200), it was found that the preferred orientation is shifted to another direction with the decrease of film thickness. In thinner film, as in Figure 1(e), the intense reflection of (200) plane in the vertical arc disappears and shifts to another azimuthal angle. The changes of orientation seem gradual with the decrease of film thickness. Although the (200) reflection at the vertical center could still be observed in the diffraction pattern [Fig. 1(e)], it is much weaker than in the thicker films [Fig. 1(b–d)]. It was analyzed that the *a* axes of the orthorhombic PE crystals developed in those thin and ultrathin films are preferentially tilted by 36° with respect to the normal direction of substrate plane, as shown in Figure 1(e). In the GIXRD pattern of 52-nm thick film [Fig. 1(f)], the *a* axes of the crystals are oriented in two different directions at the azimuthal angles of 36° and 44° from the vertical center of GIXRD patterns, while the trace of the reflection can be still observed in the vertical axis passing through the reflected main beam. As the thickness of the film becomes thinner from 115 to 21 nm [Fig. 1(e,g)], the (200) reflection

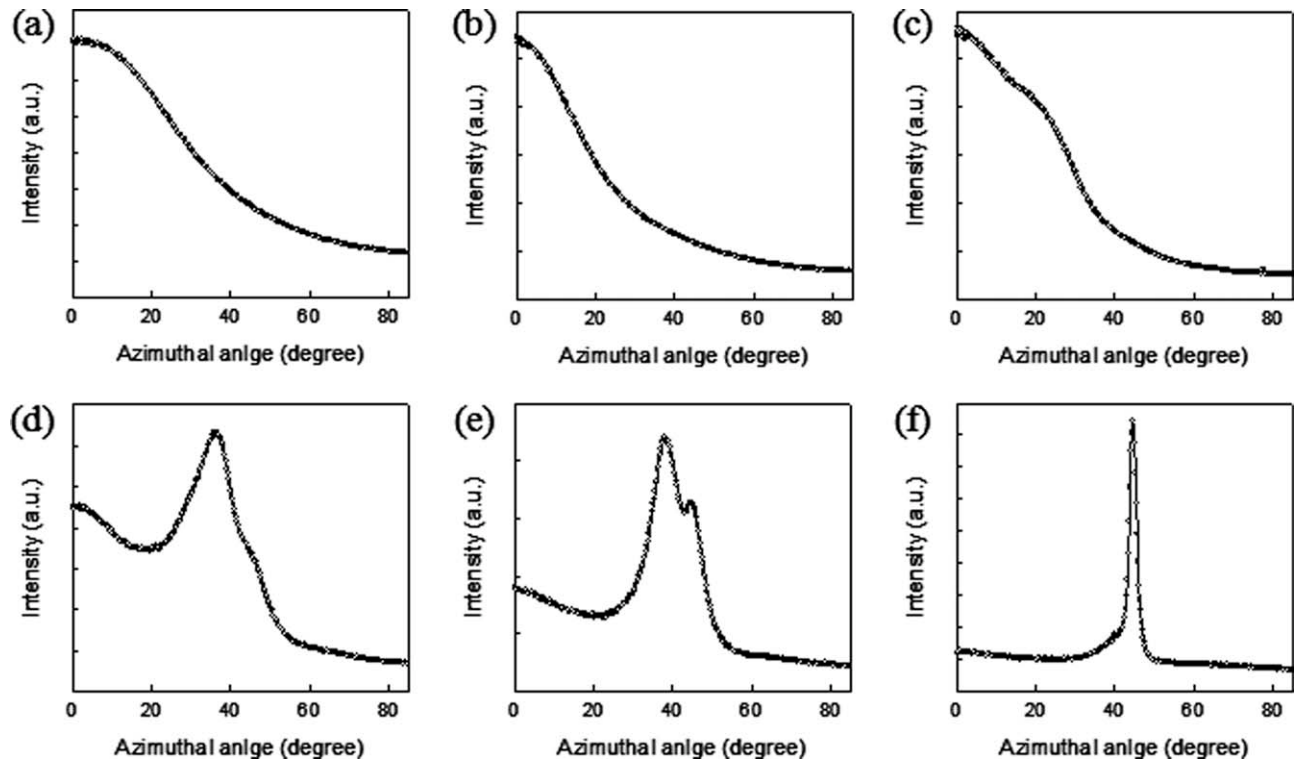

Figure 2 Azimuthal scanning profiles of (200) reflection from GIXD patterns of linear PE films. The thickness of each film was found to be (a) 1.2 μm, (b) 607 nm, (c) 255 nm, (d) 115 nm, (e) 52 nm, and (f) 21 nm, respectively In the distribution, the azimuthal angle was defined as the deviation from vertical line that passes through the reflected main beam.

appeared at an azimuthal angle of 36° becomes more intense and then gets weaker. In the mean time, the reflection at an azimuthal of 44°–46° was getting stronger, whereas the reflection at the vertical center (azimuthal angle of 0°) was almost disappeared. In the film thickness of 21 nm [Fig. 1(g)], its intensity at an azimuthal angle of 36° diminishes quite a bit, and (200) reflections cannot be found any longer. Throughout the whole samples, the (110) reflections are getting sharper with the decrease of film thickness. Therefore, it is found that the distribution of crystal orientation becomes narrower, as the thickness of the film goes thinner. Also, the shift of preferred orientation in thinner film appeared distinctively on the GIXRD patterns. The dot-like diffraction patterns were observed in thinner films, as can be seen in Figure 1(e–g). The dot-like diffraction patterns, in the reflection of both (110) and (200), denote that the crystals in these thinner films are more preferentially oriented, as compared with the thicker films.

The crystal orientations and their distribution in the films were confirmed from the azimuthally scanned profiles of (200) reflections in GIXRD patterns, as shown in Figure 2. It is quite distinctive in the azimuthally scanned profiles that the preferred orientation of crystal is shifted on the decrease of film thickness. In the scanning, the azimuthal angle was defined as the degree of deviation from vertical line with the center of reflected main beam. As has been depicted in the 2D diffraction patterns, the (200) reflection appeared on the vertical line in thick films [Fig. 2(a–c)]. Then, it shifts to $\sim$ 36° with a shoulder around 44–46° with discernable decrease of intensity at the zero azimuthal angle in thinner films [Fig. 2(d,e)]. As the degree of confinement goes stronger, eventually the diffraction $\sim$ 36° survives with a very weak intensity and sharp reflection at an azimuthal angle around $\sim$ 45° remains [Fig. 2(f)]. The azimuthal intensity distribution of (110) reflections were also changed with the decrease of film thickness. For thicker films [Fig. 3(a–c)], the (110) peak maximum located at azimuthal angle of $\sim$ 60° from the vertical center of GIXRD patterns. The results mean that, from the calculation on the basis of the geometry between the two lattice planes of (110) and (200), the *b* axis of the orthorhombic PE crystal in thin films is parallel to the substrate plane. The (110) peak moved to slightly larger azimuthal angle and appeared around 64°–66° for thinner films [Fig. 3(d–f)]. It is also observed that the azimuthal scan of (110) reflections are also getting sharper and narrower with the decrease of film thickness. It implicates again that the stronger constraint along the thickness of the film makes the distribution of crystal orientation narrower.

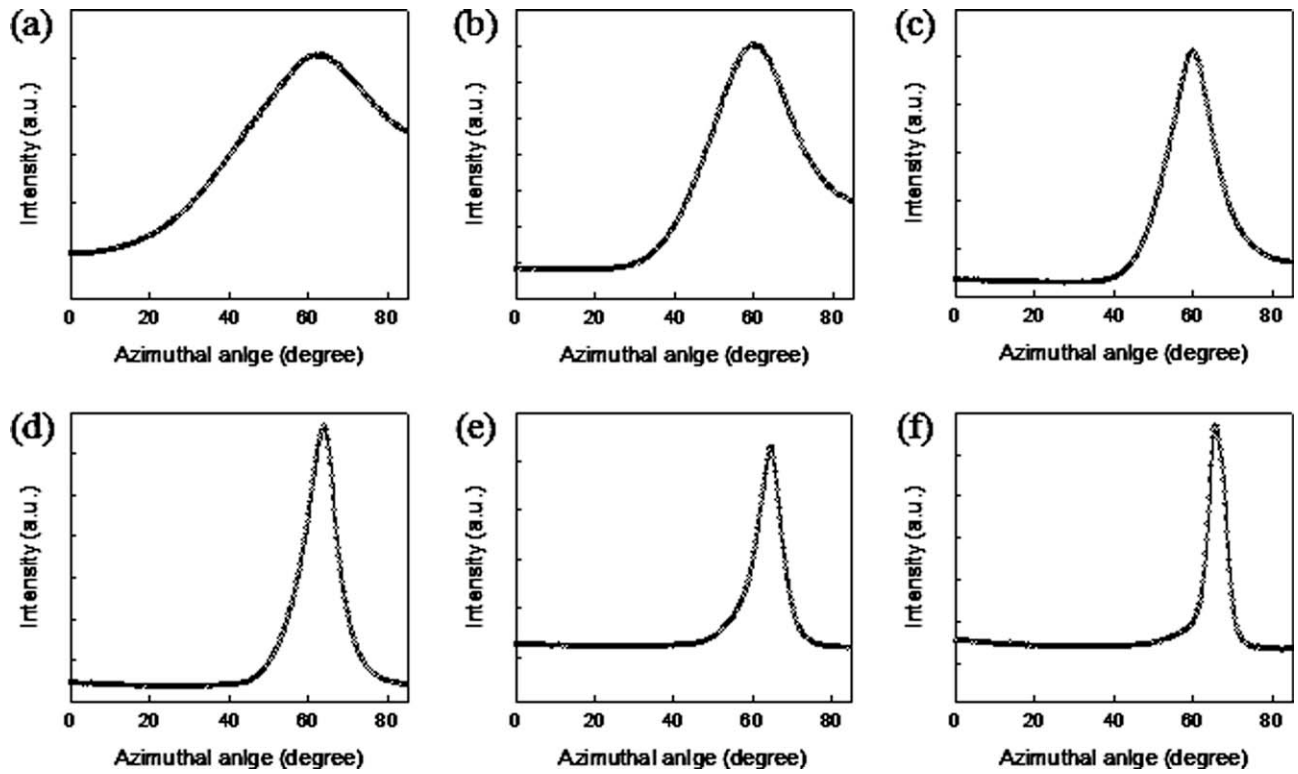

Figure 3 Azimuthal distributions of (110) reflection in GIXD patterns of linear PE films. The thickness of each film was found to be (a) 1.2 μm, (b) 607 nm, (c) 255 nm, (d) 115 nm, (e) 52 nm, and (f) 21 nm, respectively.

It was interesting that 2D spherulitic crystalline boundary was observed in thicker films despite the anisotropic crystal orientation observed in GIXRD [Fig. 1(b,c)]. The AFM topographic images of the PE films on Si substrates are shown in Figure 4. The 1.2 μm and 607 nm-thick films have 2D spherulitic grain boundary [Fig. 4(a,b)], while their GIXRD patterns represent oriented lamellar crystals. From the two different characterization methods that depict the crystalline structure in different scale, it could be found that crystallization in these thick films proceeds mainly by crystal growth starting from nucleation points, similar to bulk, and forms crystalline grain boundary, while the lamellae have preferred orientation. It is also noteworthy that the 2D spherulitic grain boundary of crystallites in these films seems to be diffuse, and eventually the grain boundary disappears with the decrease of film thickness [Fig. 4(c)]. The occurrence of blurry grain boundary [Fig. 4(a,b)] is thought to be partially due to the slow crystallization. The slow crystallization process used in this study might make the crystallites penetrate the neighboring crystal domains. Probably due to the slow crystallization process, more open crystalline structures such as sheaf-like structures for the 115- and 52-nm-thick film [Fig. 4(d,e)] and dendrite-like structures for the 21-nm-thick film [Fig. 4(f)] were thought to be observed. But, apart from the slow crystallization, this morphological difference upon the variation of the thickness indicates that the crystal orientation was affected by the confinement imposed along the direction of film thickness. The morphology of the 21-nm-thick film [Fig. 4(f)] is different from the aggregates of edge-on lamellae of the as-cast films with similar thickness, as reported elsewhere.[10,25] For the 21-nm-thick PE film, flat and wide crystalline structures were observed. It seems not difficult to identify that the flat area in the AFM surface image is flat-on lamellae.

Combining the information from the GIXRD analysis and the AFM surface observation of the PE films, the thickness-dependent orientation of lamellae in PE films on Si substrates was schematically drawn in Figure 5. The schematic illustration was drawn on the basis of assumption that the lamellar normal is tilted from the *c* axis of the crystal at an angle about $\sim 30^\circ$ that is known for crystal grown in solution.[34] In cases of the thicker films (thickness $\sim$ 1.2 μm, 607 nm, 255 nm), the edge-on lamellae were mainly formed (top illustration of Fig. 5). Even the 2D spherulitic crystalline grain boundary was observed at the same time (thickness $\sim$ 1.2 μm and 607 nm). For the PE films with intermediate thickness (thickness of 115 and 52 nm), the flat-on lamellae or slightly inclined flat-on lamellae were dominantly developed, as represented in the second and third illustrations from the top in Figure 5.

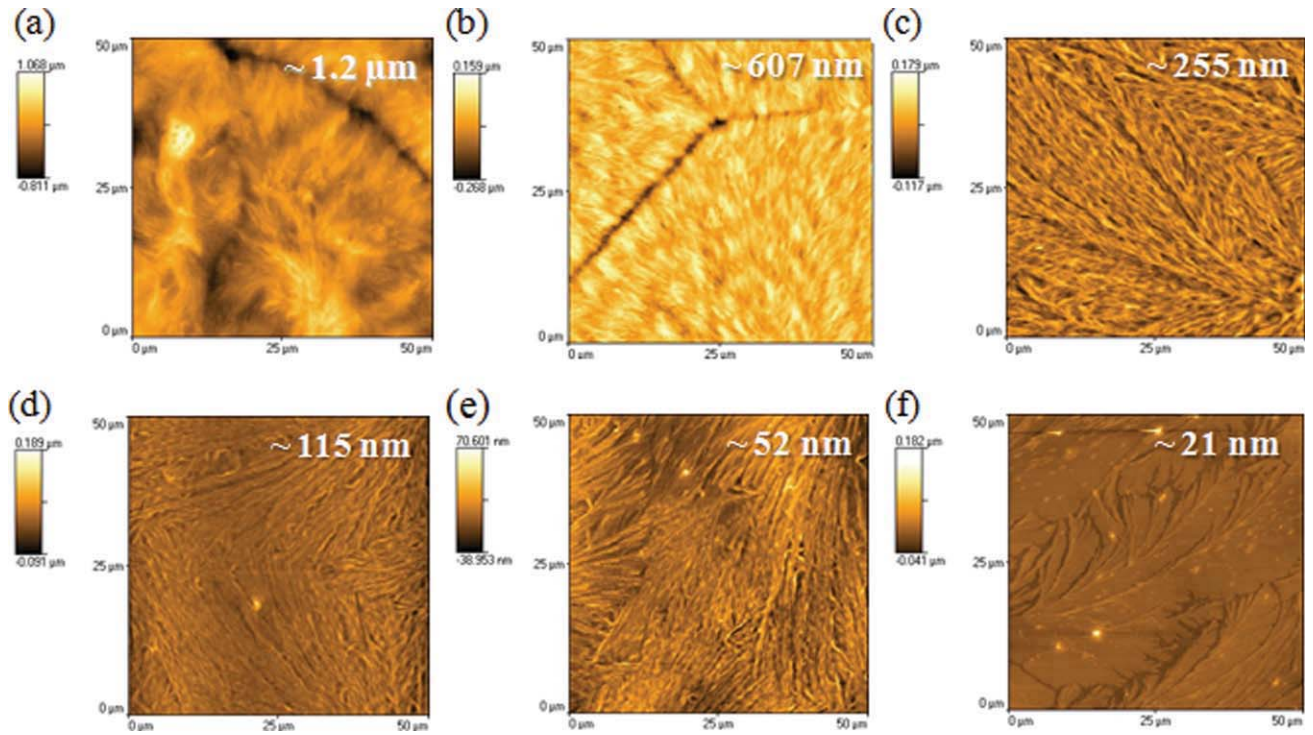

Figure 4 AFM height images of linear PE films on Si ⟨100⟩ wafers with the thickness of (a) 1.2 μm, (b) 607 nm, (c) 255 nm, (d) 115 nm, (e) 52 nm, and (f) 21 nm. [Color figure can be viewed in the online issue, which is available at wileyonlinelibrary.com.]

However, the edge-on lamellae still existed in this range of thickness of film, although the population of them was getting minor with the decrease of film thickness. It can be confirmed from the existence of weak intensity distribution for the (200) reflection in GIXRD around the azimuthal angle of 0° in Figure 1(e,f). It indicates that gradual change of the dominant lamellar orientation from edge-on to flat-on occurs with the decrease of film thickness due to the more severely imposed confinement. It is also worthy to mention that the edge-on lamellar orientation with broad distribution exhibited in the thicker PE films (thickness ~ 1.2 μm, 607 nm, and 255 nm), while the lamellae with different orientations mainly coexisted in the thinner films (thickness ~ 115 and 52 nm). When the film becomes much thinner, the crystal was aligned along a preferred orientation. In the thinnest film of this study (21-nm-thick film), flat-on orientation of lamellar crystal was dominantly observed, and the schematic illustration of crystal orientation is given in the bottom of Figure 5.

Judging from the results above, the crystalline orientation and crystalline morphology in thin PE films were strongly dependent on the film thickness. In the PE films over hundreds of nanometer thick, crystalline grain boundary with rather preferred orientation of crystal but with some orientation distribution was developed, unlike the bulk random orientation. The grain boundary means that the crystalline structures were formed via mainly lateral growth after nucleation with the preferential orientation of the lamellae. But, the morphology was changed into more distinctive preferential appearance of flat-on lamella with the decrease of film thickness. It looks much related to the thickness of PE film, or degree of confinement, to make the specific orientation in thin films. As the thickness of the film goes thinner, the whole film is thought to be under the influence of substrate surface. When the crystallization happened under the environment where edge-on lamella were formed majorly by the benefit of substrate surface,[33] from the energetic point of view, the interfacial free energy reduces the total energy of crystal. Therefore, the extra stability given by substrate is thought to drive the preferred orientation of lamellar crystal during the crystallization in the thick film within this thickness range. However, formation of edge-on lamellae would become less favorable with the decrease of film thickness.[12] As the film gets thinner, the width of edge-on lamellae would go narrower. The narrowing of the crystal would induce the instability of lamellae, because the fraction of unstable interfaces (i.e., surface-to-volume ratio) increases.[34] Thus, it is conjectured that formation of edge-on crystal is not energetically favored any more with less than a certain thickness, and other crystalline structure might appear dominantly. In a much thinner film, the entropy penalty driven by the degree of confinement seems to be the determining factor in the

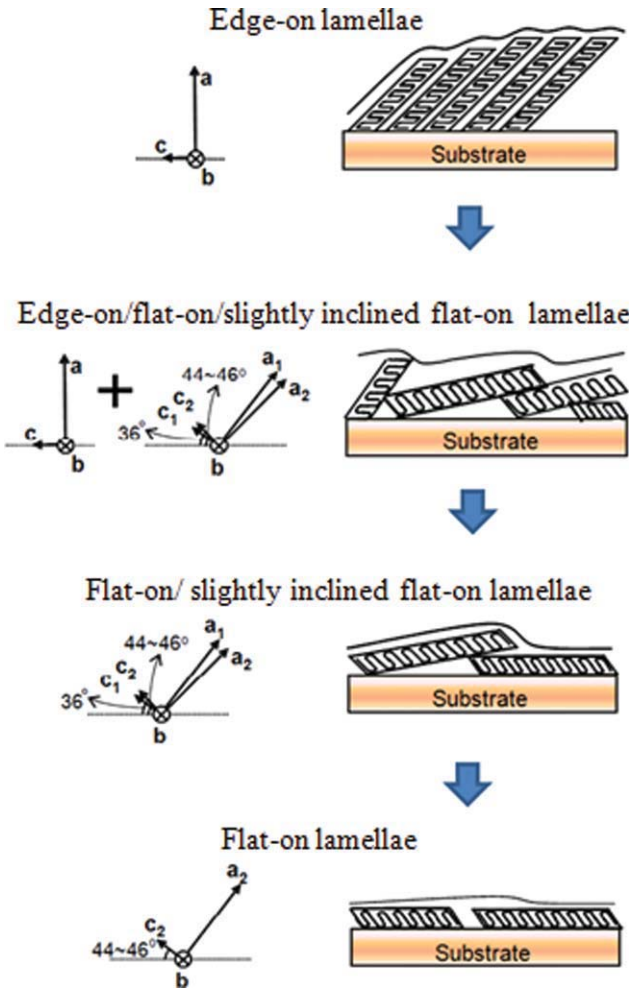

Figure 5 Schematic representations of gradual change of lamellar orientation upon the variation of film thickness based on the GIXD analysis and AFM experiment. The lamellae and the lattice vectors in linear PE films are denoted on the decrease of the film thickness from top to bottom. [Color figure can be viewed in the online issue, which is available at wileyonlinelibrary.com.]

formation of lamellar crystal. In the thinner film, flat-on crystals were majorly formed. It is clear that the formation of flat-on lamella does not have any energetic benefit from the substrate surface, and thus it can have no more advantages in the light of its overall energy. So, it is guessed that this orientation change happened due to the confinement in this thickness range, and the crystallization process and the crystal orientation was governed probably kinetically under the strong constraint. The overall crystallization in this range of film thickness should be dominated by the crystal growth, judging from the fact that lamellar morphology was still observed as mentioned above.

It was interesting that we could observe the systematic changes of crystal orientation in thin PE films with different thickness via GIXRD. The existence of slightly inclined lamella implies that the crystalline structure and its formation could be strongly influenced by the constraint rather than the energetic benefit from the substrate in ultrathin films. Considering that the slightly inclined lamella appeared in the middle of orientation change from edge-on to flat-on upon the variation of the degree of confinement, and it could coexist with flat-on lamella, it is valid to contend that the crystallization of linear PE is governed by the strong confinement in ultrathin polyethylene film. In this ultrathin film, it seems quite obvious that the energetic gain owing to the interface cannot compensate for the entropy penalty driven by the degree of confinement any more, and the crystal formation is dictated by the film thickness. We also conjecture that the origin of the coexistence of the flat-on lamellae and slightly inclined flat-on lamellae in thinner film might be the twisting nature of PE lamellae due to the unbalanced surface stress.[32] However, it seems clear to have an idea that the crystalline structures would be more influenced by the constraint imposed by film thickness, and that confinement may induce the kinetic formation of large flat-on lamella rather than edge-on crystal under a suitable environment.

CONCLUSION

In summary, we observed that the crystal orientation and the lamellar morphology in the linear PE films on the Si substrates changed upon the variation of film thickness. We found that the lateral confinement due to the film thickness can induce the formation of large flat-on lamellae rather than edge-on lamellae with small width. Taking the benefit of GIXRD, we could observe the systematic crystal orientation changes and newly found that the flat-on lamellae with slight inclination were formed and they coexisted with the flat-on lamellae with the preferred in-plane orientation in ultrathin film. This result is evidence that the crystallization of lamella in a much thinner film is more strongly influenced by the degree of confinement rather than energetic benefit of substrate surface.

It is grateful that Guiduk Yu, Kyunghee Lee, and Bongseok Kim performed the experimental GIXRD measurement. The experimental support at 4C2 beamline of PLS is also gratefully acknowledged.

References

1. Frank, C. W.; Rao, V.; Despotopoulou, M. M.; Pease, R. F. W.; Hinsberg, W. D.; Miller, R. D.; Rabolt, J. F. Science 1996, 273, 912.
2. Despotopoulou, M. M.; Frank, C. W.; Miller, R. D.; Rabolt, J. F. Macromolecules 1996, 29, 5797.
3. Despotopoulou, M. M.; Miller, R. D.; Rabolt, J. F.; Frank, C. W. J Polym Sci B Polym Phys 1996, 34, 2335.
4. Cho, K. W.; Kim, D. W.; Yoon, S. Macromolecules 2003, 36, 7652.

5. Keddie, J. L.; Jones, R. A. L.; Cory, R. A. Faraday Discuss 1994, 98, 219.
6. Forrest, J. A.; Dalnoki-Veress, K.; Dutcher, J. R. Phys Rev E 1997, 56, 5705.
7. Reiter, G. Phys Rev Lett 1992, 68, 75.
8. Li, G.; Shrotriya, V.; Huang, J. S.; Yao, Y.; Moriarty, T.; Emery, K.; Yang, Y. Nat Mater 2005, 4, 864.
9. Newman, C. R.; Frisbie, C. D.; da Silva, D. A.; Bredas, J. L.; Ewbank, P. C.; Mann, K. R. Chem Mater 2004, 16, 4436.
10. Mellbring, O.; Oiseth, S. K.; Krozer, A.; Lausmaa, J.; Hjertberg, T. Macromolecules 2001, 34, 7496.
11. Hu, Z. J.; Huang, H. Y.; Zhang, F. J.; Du, B. Y.; He, T. B. Langmuir 2004, 20, 3271.
12. Wang, Y.; Ge, S.; Rafailovich, M.; Sokolov, J.; Zou, Y.; Ade, H.; Luning, J.; Lustiger, A.; Maron, G. Macromolecules 2004, 37, 3319.
13. Schonherr, H.; Frank, C. W. Macromolecules 2003, 36, 1188.
14. Wang, J.; Lu, G.; Li, L.; Lu, Z.; Yang, X.; Zhou, E. Macromolecules 2008, 41, 1273.
15. Reiter, G.; Sommer, J. U. Phys Rev Lett 1998, 80, 3771.
16. Taguchi, K.; Miyaji, H.; Izumi, K.; Hoshino, A.; Miyamoto, Y.; Kokawa, R. Polymer 2001, 42, 7443.
17. Mareau, V. H.; Prud'homme, R. E. Macromolecules 2002, 35, 5338.
18. Massa, M. V.; Dalnoki-Veress, K.; Forrest, J. A. Eur Phys J E 2003, 11, 191.
19. Woo, E.; Huh, J.; Jeong, Y. G.; Shin, K. Phys Rev Lett 2007, 98, 136103.
20. Steinhart, M.; Goring, P.; Dernaika, H.; Prabhukaran, M.; Gosele, U.; Hempel, E.; Thurn-Albrecht, T. Phys Rev Lett 2006, 97, 027801.
21. Shin, K.; Woo, E.; Jeong, Y. G.; Kim, C.; Huh, J.; Kim, K. W. Macromolecules 2007, 40, 6617.
22. Loo, Y. L.; Register, R. A.; Ryan, A. J. Phys Rev Lett 2000, 84, 4120.
23. Shin, K.; Xiang, H. Q.; Moon, S. I.; Kim, T.; McCarthy, T. J.; Russell, T. P. Science 2004, 306, 76.
24. Pearce, R.; Vancso, G. J. Macromolecules 1997, 30, 5843.
25. Bartczak, Z.; Argon, A. S.; Cohen, R. E.; Kowalewski, T. Polymer 1999, 40, 2367.
26. Keith, H. D.; Padden, F. J.; Lotz, B.; Wittmann, J. C. Macromolecules 1989, 22, 2230.
27. Zhu, L.; Cheng, S. Z. D.; Calhoun, B. H.; Ge, Q.; Quirk, R. P.; Thomas, E. L.; Hsiao, B. S.; Yeh, F. J.; Lotz, B. J Am Chem Soc 2000, 122, 5957.
28. Wang, Y.; Rafailovich, M.; Sokolov, J.; Gersappe, D.; Araki, T.; Zou, Y.; Kilcoyne, A. D. L.; Ade, H.; Marom, G.; Lustiger, A. Phys Rev Lett 2006, 96, 028303.
29. Fromsdorf, A.; Woo, E. M.; Lee, L. T.; Chen, Y. F.; Forster, S. Macromol Rapid Commun 2008, 29, 1322.
30. Ho, R. M.; Lin, C. P.; Hseih, P. Y.; Chung, T. M.; Tsai, H. Y. Macromolecules 2001, 34, 6727.
31. Factor, B. J.; Russell, T. P.; Toney, M. F. Macromolecules 1993, 26, 2847.
32. Lotz, B.; Cheng, S. Z. D. Polymer 2005, 46, 577.
33. Bartczak, Z.; Argon, A. S.; Cohen, R. E.; Kowalewski, T. Polymer 1999, 40, 2367.
34. Gedde, U. W. Polymer Physics; Chapman and Hall: New York, 1995; Chapter 7.